THE ASTRONOMICAL JOURNAL VOLUME 112, NUMBER 3 SEPTEMBER 1996

THE POSITION OF THE NUCLEUS AND THE NATURE OF THE ALIGNED COMPONENT IN 3C 368

ALAN STOCKTON, SUSAN E. RIDGWAY,[1] AND MELINDA KELLOGG[2]

Institute for Astronomy, University of Hawaii, 2680 Woodlawn Drive, Honolulu, Hawaii 96822
Electronic mail: stockton@ifa.hawaii.edu, s.ridgway1@physics.oxford.ac.uk, mk@astro.caltech.edu

Received 1996 April 5; revised 1996 June 6

ABSTRACT

We present deep spectroscopy and high-resolution IR images of the $z=1.132$ radio galaxy 3C 368. The spectroscopy was obtained with LRIS on the Keck I telescope. It shows a complex velocity structure in the emission lines, with brightness enhancements corresponding with excursions of amplitude up to 1500 km s^{-1} to higher or lower velocities from a faint, low-velocity "backbone," which may indicate the quiescent outflow pattern. High velocities are correlated with strong emission lines, indicating a connection between the acceleration process and the excitation of the emission. We consider the possibility that the high velocity gas may be due to superwinds from radio-jet-induced starbursts, but we show from energetic considerations that the required mass in young stars is probably inconsistent with the observed continuum. While simple entrainment alone cannot account for the high velocities, it seems almost certain that they arise in some way from the direct interaction of radio jet (or thermal matter entrained in it) with the ambient gas. In the brightest aligned component, we find that about 80% of the UV continuum just beyond the Balmer limit is due to thermal emission from the nebular gas. If previous measurements of $\gtrsim 10\%$ polarization in this region are correct, the true polarization of the residual after removal of the (presumably unpolarized) nebular continuum would be $\gtrsim 50\%$. However, there are ambiguities in the polarization data and some recent observations show little or no polarization. Finally, our spectroscopy leaves no doubt that Hammer *et al.* [ApJ, 374, 91 (1991)] have correctly identified what was long supposed to be the nucleus of 3C 368 as a projected Galactic M star. Our IR images show that the true nucleus lies $\sim 1\farcs5$ N of the star and is not coincident with any feature prominent in the optical images.

1. INTRODUCTION

3C 368 has, in many ways, the most extreme properties of any of the $z\sim 1$ radio galaxies in the 3CR catalogue. It has the strongest emission-line spectrum, one of the bluest optical colors, and the most striking alignment between the optical continuum and the radio emission. It was one of the first objects to present a compelling warning that powerful radio galaxies at high redshift show qualitative differences from their lower-redshift (and lower-radio-power) cousins (e.g., Spinrad 1982).

Because of its extreme properties, 3C 368 has been the object of a number of detailed investigations (Djorgovski *et al.* 1987, 1990; Hammer *et al.* 1991; Rigler *et al.* 1992; Meisenheimer & Hippelein 1992). Here we present and discuss very deep spectroscopy obtained with LRIS on the Keck I telescope, a deep K' image obtained with NIRC on Keck I, and a high-resolution IR image obtained with the 1024×1024 QUIRC IR Camera and fast-guiding tip-tilt secondary on the 2.2 m University of Hawaii telescope.

2. OBSERVATIONS

2.1 Spectroscopy

The spectra were obtained with the Low-Resolution Imaging Spectrometer (LRIS) of the Keck I telescope. We used the 300 groove mm^{-1} grating, blazed at 5000 Å, with an OG 570 order-separating filter to give a dispersion of 2.48 Å $pixel^{-1}$ and a useful wavelength range of 5700–9500 Å. The slit (1″ wide, projecting to ~5 pixels on the Tektronix 2048×2048 CCD) was oriented at PA 13°.3 and aligned on a conveniently-positioned star ~13″ S of 3C 368. We obtained a total of 9600 s of exposure; the sky was mostly clear, with intermittent thin cirrus. We monitored the seeing by measuring star profiles from the slit-viewing camera: the FWHM varied between 0″.6 and 0″.7. The spectra were reduced using standard IRAF routines to give a final calibrated two-dimensional spectrum, with a linear wavelength scale and with distortions in the spatial coordinate removed. We have extracted and summed along the spatial axis subsets of this image corresponding to various morphological components in the galaxy.

2.2 IR Imaging

We present two IR images of 3C 368. One is a K'-band image obtained on 1995 March 20 with the Keck I Near-Infrared Camera (NIRC), which employs a 256×256 InSb

[1]Current address: Physics Department, Oxford University, Keble Road, Oxford, OX1 3RH, UK.
[2]Current address: Astronomy Department, Califonria Institute of Technology, 105-24, Pasadena, CA 91125.

 0004-6256/96/112(3)/902/7/$10.00

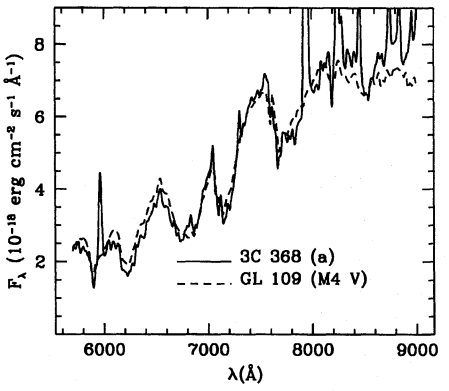

FIG. 2. Spectrum of component *a*. The spectrum of the M4 V star GL 109 is superposed.

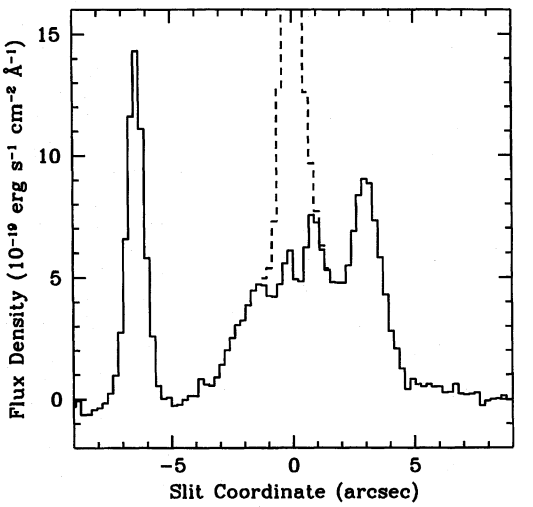

FIG. 3. The continuum profile of 3C 368, summed from line-free regions of the spectrum: *dashed line*—total profile; *solid line*—profile with M star removed.

array. The images were affected by wind shake and had FWHM of 0.″6×0.″9. The second IR image was obtained with QUIRC, an IR camera incorporating a Rockwell 1024×1024 HdCdTe array, on the University of Hawaii (UH) 2.2 m telescope. The telescope was in its *f*/31 configuration, where the secondary mirror is mounted on a Polytec piezo-electrically driven platform, which allows the mirror to be tilted in two coordinates in response to image motion error signals received from a fast-readout CCD on the guide probe at the focus. The scale at the IR detector was 0.″06 pixel^{-1}; in order to achieve as high an illumination of the detector as possible, we used a special $H+K$ filter, provided by Len Cowie and Esther Hu. This filter has high transmission in the H and K bands, but it is notched in the low-transmission region between the two in order to minimize background.

For both data sets, we used an iterative technique to remove the sky background, flat-field, register, and combine the images. The UH observations were registered onto a grid of 0.″03 pixels. The recorded FWHM of the individual 180 s images varied from 0.″26 to 0.″38 over the 7200 s of total integration we obtained. Our final combined image has a FWHM of 0.″32.

3. RESULTS

Figure 1 (Plate 36) shows a montage consisting of an optical *HST* image of 3C 368 [previously published by Longair *et al.* (1995), and kindly supplied to us by Malcolm Longair and Phillip Best], our high-resolution $H+K$ image, our Keck I K' image, and two versions of our Keck LRIS spectral image of the [O II] λ3727 line emission. We have retained the designations of components *a*, *b*, and *e* of Hammer *et al.* (1991) and Rigler *et al.* (1992). Our new designations (*d*, *f*, and *i*) attempt to avoid conflicts with other previously-defined components.

3.1 The Projected Galactic M Star

The brightest component (*a* in Fig. 1) was long assumed to be the nucleus of 3C 368, and the radio maps of Djorgovski *et al.* (1987) and Chambers *et al.* (1988) show weak radio components at this position. However, Hammer *et al.* (1991) have shown spectroscopically that this object is likely a projected Galactic M-dwarf star. This suggestion was supported by the colors found by Rigler *et al.* (1992), and by the fact that the recent 3.6-cm map of Longair *et al.* (1995) does not show a radio component at this position. Our spectrum of this object, shown in Fig. 2, should satisfy any lingering doubt on this matter: the spectrum is clearly that of an M4 or M5 star at zero redshift.

3.2 The Position of the Nucleus

After the projected M star is discounted, the component with the highest optical continuum surface brightness is the northern knot (*b*). Hammer *et al.* in fact identify this object as the probable nucleus, principally on the basis of its strong emission and the velocity dispersion in the emission lines. However, most of the total flux is in a diffuse, elongated background component aligned with the radio axis. The continuum profile shown in Fig. 3 was obtained by summing (in wavelength) the line-free continuum regions of the spectrum between roughly 2800 and 3700 Å. This profile is fairly symmetric about the bright emission knot (*e*) ~0.″8 N of the M star, lending some support to the suggestion of Longair *et al.* (1995) that the nucleus is coincident with that object.

However, we believe that the true nucleus actually lies *between* these two suggested identifications. Our IR images show that the brightest component (*i*) near rest-frame 1 μm lies about ~1.″5 N of the M star, near a relative minimum in the optical brightness distribution, coincident with object *K* of Djorgovski *et al.* (1990), and we believe this apparently highly-reddened component to be the nucleus. A similar situation exists for 3C 324, where the IR peak identified with the nucleus lies in a region between optical peaks (Dickinson *et al.* 1996).

3C 368 has been cited as a prime example of a high-redshift radio galaxy for which the well-known alignment of

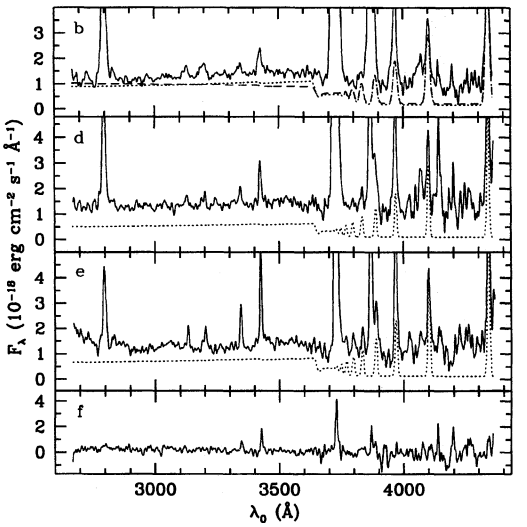

FIG. 4. Spectra of components of 3C 368. Lines can be identified by reference to Table 1. The dotted trace gives the thermal nebular continuum for 10,000 K in the low-density limit, assuming He is 10% ionized. The dashed trace shown with component *b* is the same, for 15,000 K. The spectra have been de-redshifted, but the flux densities are given in the observed frame.

TABLE 1. Line intensities in 3C 368 components.

Line	*b*	*d*	*e*	*f*
Mg II λ2798	23.2	17.2	9.8	1.4
O III λ3133	2.2	1.3	1.4	···
He II λ3203	3.5	1.8	2.4	···
[Ne V] λ3346	2.1	1.8	3.2	1.7
[Ne V] λ3426	4.6	3.6	7.1	3.2
[O II] λ3727	181.	176.	85.5	9.2
[Ne III] λ3869	28.1	23.5	27.4	4.1
Hζ λ3889	9.9	6.6	6.0	···
[Ne III] λ3967 + Hε λ3970	16.6	13.1	16.1	···
[S II] λ4069 + [S II] λ4076	5.8	5.6	1.8	···
Hδ λ4101	12.2	9.2	8.4	···
Hγ λ4340	23.4	19.4	20.2	···

Notes to TABLE 1

Line intensities are in units of 10^{-17} erg cm^{-2} s^{-1}. Typical errors (1σ) for unblended features in the first three columns are ~0.4 (or ~10% for the stronger lines) for wavelengths <4000 Å, and ~1 (or ~10%) for longer wavelengths. For component *f*, the errors are ~0.2 (or ~10%).

the optical continuum with the radio structure (the "alignment effect:" Chambers *et al.* 1987; McCarthy *et al.* 1987) persists strongly into the IR (Chambers *et al.* 1988; Djorgovski *et al.* 1990). We note that eliminating the M star from the picture and identifying component *i* with the nucleus weakens both the amplitude and the accuracy of alignment of the IR structure, but the IR alignment effect is still clearly recognizable in this object.

3.3 Emission-Line Spectra

We show the spectra of various components of 3C 368 in Fig. 4, and we identify the lines and give their strengths in Table 1. The ionization varies greatly from region to region. It is highest in the region of faint emission (*f*) beyond the N extent of the galaxy seen in the deepest continuum images, in the vicinity of the N radio lobe and extending somewhat beyond it. Here, [Ne V] λ3426 is nearly half as strong as [O II] λ3727 and almost equal in strength to [Ne III] λ3869. The ionization, though less, is still fairly high in knot *e*; it is much lower in *b* and in the general diffuse component *d*, in which we have included the region between *b* and *e*, and all of the emission to the south of the M star *a*. The emission-line ratios we have observed are generally consistent with photoionization by a flat UV continuum (e.g., a hidden quasar nucleus) or by a hot thermal source, such as the continuum produced in high-velocity shocks (e.g., Dopita & Sutherland 1996). However, the high ionizations in regions *e* and *f* are unusual. They are almost identical (over the spectral region we have observed) to those found by Lacy & Rawlings (1994) in their knot *a* associated with the $z = 1.079$ radio galaxy 3C 356. Lacy and Rawlings stress that (in its spectral characteristics), 3C 356*a* "is quite unlike any of the well-known classes of active galaxy." By fitting ionization models to their spectra, which include a much wider wavelength coverage than we have, they conclude that the most likely source of ionization is photoionization by a $\sim 10^7$ K thermal continuum produced in high-speed shocks. These plausibly result from the impact of cloudlets entrained in the radio jet on ambient clouds of gas.

This conclusion may have some corroboration from a feature of both our spectra and of other recent high-S/N spectra of $z \sim 1$ radio galaxies (e.g., Lacy & Rawlings 1994, Dickinson *et al.* 1996): the near-equality of the intensities of the Bowen fluorescence O III λ3133 line and He II λ3203. Under a wide range of physical parameters, plausible power-law photoionizing continua produce O III λ3133/He II λ4686 ratios $\gtrsim 5$ (Netzer *et al.* 1985), which correspond to O III λ3133/He II λ3203 ratios of $\gtrsim 12$. Because of the origin of the Bowen fluorescence in pumping by He II Lyα, the only ways to alter this ratio are (1) to alter the relative strengths of He II Lyα and the other He II recombination lines (e.g., via radiative transfer effects or dust intermixed in the He II region); or (2) to change the Bowen conversion efficiency, i.e., the fraction of He II photons that actually result in emission in the Bowen O III lines. This efficiency could be decreased by lowering the metallicity, although the models of Netzer *et al.* indicate that abundance variations may be strongly buffered: two otherwise identical models with metallicities differing by a factor of 16 show only a factor of 2 difference in the O III/He II ratio. It appears that the most likely way in which the Bowen efficiency could be lowered to produce line ratios like those we observe is to increase the ionization so that most of the oxygen in higher ionization states than O III: this means either increasing the ionization parameter or the "hardness" (i.e., lower spectral index or higher temperature) of the ionizing radiation. It is very difficult to obtain the required ionization with plausible power-law models, where the radiation is produced in a hidden quasar nucleus, because spectral indices are typically $\alpha \sim 1$ (where $f_\nu \sim \nu^{-\alpha}$), and because of the large dilution factors involved. On the other hand, the required ionization level could be achieved fairly

naturally from a 10^6–10^7 K thermal continuum in close proximity to the emitting regions. This would be roughly what one would expect from ~500 km s^{-1} shocks.

3.4 Nebular Thermal Emission and the Blue Aligned Continuum

Dickson *et al.* (1995) have recently re-emphasized that, in sources with strong emission lines, the thermal nebular continuum emission component can be appreciable. They include the northern component *b* of 3C 368 among the three examples they discuss, but, since their spectrum does not allow a measurement of any of the stronger Balmer emission lines, they calculate the thermal continuum from an assumed ratio of Hβ to [O II] λ3727 and an electron temperature of 15,000 K. We have both Hγ and Hδ in our spectra, so we can anchor the scaling of the thermal continuum to the Balmer emission lines, assuming case B (see, e.g., Aller 1987 or Osterbrock 1989). We include the He I and He II continua as well, making the arbitrary but conservative assumption that 10% of the He is ionized (if all of the He were ionized, the near-UV thermal continuum would be roughly twice that of H alone, whereas if it were essentially all neutral, the continuum would only be about 10% higher than that of H alone). We assume the low-density limit in calculating the two-photon emission. Figure 4 shows our spectrum of *b* with models of this nebular thermal continuum for electron temperatures of 10,000 and 15,000 K. Note that for the higher temperature, the continuum remaining after subtracting the nebular thermal component would drop steeply beyond the Balmer limit and essentially go to zero near 2800 Å. This behavior seems difficult to reconcile with most plausible sources for this continuum, given that old stars seem ruled out by the lack of evidence for a 4000 Å break. We therefore favor a lower temperature of around 10,000 K, which leaves a residual continuum that is closer to being flat in F_λ. In component *b*, the thermal nebular continuum accounts for ~80% of the total continuum beyond the Balmer limit. Figure 4 also shows components *e* and *d* with 10,000 K thermal nebular spectra superposed; in these regions, the nebular continuum comprises a smaller, but still significant, fraction of the total.

3.5 Velocity Structure in the [O II] Emission

The two lower panels of Fig. 1 show two versions of the two-dimensional spectral image of the [O II] λ3727 line. The left-hand one shows the combined image as observed; the right-hand one shows a Lucy-Hook deconvolution of this image, where the point-spread-function kernel has been constructed from a line profile of a night-sky line in the dispersion direction and the profile of a star on the slit in the spatial direction. Because of the relatively high S/N of the original image and the fairly good seeing during the integration, the deconvolution works well and gives new insight into the nature of the complex velocity field. There appears to be a coherent velocity pattern extending over the whole length of the region over which emission is observed, consisting of a nearly constant velocity north of the IR nucleus *i*, a lower nearly constant velocity south of *i*, and a steep velocity gradient connecting the two at *i*. However, at points where the emission-line intensity is greatest, there are often large velocity excursions to one side or the other of this basic velocity "backbone," diverting one's attention from its underlying regularity.

The flat velocity curve on either side of the nucleus and the steep gradient at the nucleus are reminiscent of the flat rotation curves present in massive disk galaxies. A symmetric velocity curve in 3C 265 recently led Dey & Spinrad (1996) to suggest that rotation dominates the gas kinematics in that galaxy. However, the alignment effect in 3C 368 suggests that, in this case, we are dealing with a truly linear structure and either infall or outflow along this axis seems more likely. In attempting to interpret the velocity structure, one would like to know which end of the galaxy is the closer; unfortunately, the radio depolarization data (Djorgovski *et al.* 1987) are somewhat ambiguous. Taken at face value, the rotation measures in the southern lobe are higher than those in the northern lobe, indicating that the latter is the closer side. However, there could be a 180° ambiguity in the N lobe rotation measures, which would then make it the more distant. This difference is crucial in deciding the nature of the underlying basic velocity structure (the "backbone"): if the N side is closer, it is infall; if the S side is closer, it is outflow. One might expect outflow to be the more likely, if the thermal gas is partly entrained by the radio jet, but we cannot confirm this supposition until the radio depolarization ambiguity is resolved.

4. DISCUSSION

4.1 The Nature of the Aligned Continuum

What is the origin and nature of the aligned component in 3C 368? There is probably no single, simple answer to this question. Previous work has emphasized the optical polarization of the extended components (di Serego Alighieri *et al.* 1989; Scarrott *et al.* 1990), which has been taken as evidence for scattering from a bright, hidden nucleus, in consonance with the unification of quasars and FR II radio galaxies (Scheuer 1987; Barthel 1989). Our conclusion that the nucleus lies in a region of high optical obscuration is consistent with this view as well, even though we do not yet see an unresolved component at rest-frame ~1 μm.

However, while scattering may play a role in the alignment effect in 3C 368, it now appears that it is neither the only nor even the dominant physical mechanism contributing. In the region just shortward of the Balmer limit, the nebular thermal continuum comprises ~50% of the aligned continuum overall, ranging up to ~80% in the brightest component, *b*. This strong dilution means that our previously-reported lack of any evidence for scattered broad Mg II λ2798 emission in our relatively high S/N spectrum of *b* (Stockton *et al.* 1995) could still be consistent with a hidden quasar nucleus in 3C 368. It also means that, if the polarization really is observed to be $\gtrsim$10% in *b*, and if scattering contributes all of the polarization, then the scattered component must have a polarization of $\gtrsim$50%. This value is at the upper end of the range of those found for dust scattering in Galactic reflection nebulae. But, for 3C 368, the de-

tails of the polarization evidence and its interpretation remain equivocal. Imaging polarimetry of these low-surface-brightness features is difficult, and resolution in ground-based observations is marginal. Such problems are evident in the polarization maps of Scarrott *et al.* (1990): in their "no filter" map, a star (near coordinates $-2''$, $2''$ in the upper-left panel of our Fig. 1) is shown to have $\sim 10\%$ polarization, as is the region of their "*V* filter" map that is dominated by flux from the M star *a*. Meisenheimer & Hippelein (1992) have expressed scepticism about both the significance of the di Serego Alighieri *et al.* (1989) measurement of polarization in 3C 368 and whether the results of Scarrott *et al.* apply to the continuum or to contaminating emission lines in the passband. Finally, very recent imaging polarimetry with *HST* and spectropolarimetry with the Keck I telescope have found no detectible polarization in any component of 3C 368, to an upper limit of ~ 2 or 3% (Dey *et al.* 1996). The main lesson is that the current polarization data are certainly not sufficient to exclude the possibility that there may be additional significant nonscattered contributions to the aligned continuum in 3C 368 in addition to the nebular scattered component.

4.2 High Velocities in the Ionized Gas

How can we account for velocities such as those seen in knot *b*, which range up to 1500 km s^{-1} from that of the apparent quiescent flow? Velocities $\gtrsim 1000$ km s^{-1} have often been noted in the extended emission regions around high-redshift radio galaxies (e.g., Spinrad & Djorgovski 1984; McCarthy *et al.* 1990; Chambers *et al.* 1990; Lacy & Rawlings 1994), so this is a general problem. Such velocities have often been attributed to entrainment by the radio jet (De Young 1986). We consider here how our 3C 368 observations can constrain the likely options.

As we indicated in Sec. *3.5*, where the velocity dispersion increases at the emission-line intensity peaks, it generally appears one sided (with respect to the "backbone"). Note that for the brightest emission region (*b*), although the predominant emission extends to lower velocities, there appears to be a much weaker mirroring of this velocity structure to higher velocities. This sort of behavior could be interpreted as an expanding cloud with embedded dust. However, a careful measurement shows that the apparent mirroring does not occur at precisely the same slit position but seems to be centered $\sim 0\farcs15$ to the S of the stronger emission, so it may be associated with a separate component. Also, the "expansion plus dust" explanation cannot apply to the weaker emission region $0\farcs7$ to the north of *b*, for which the observed velocity excursion is only to *higher* velocities.

The correlation between intensity and velocity dispersion indicates that we are seeing some sort of physical connection between the excitation in the gas clouds and the mechanism by which the gas is accelerated to high velocities. It is possible that what we have called the velocity "backbone" (the nearly-constant velocity offsets of the faint emission on either side of the IR nucleus) is due to cloudlets entrained at the boundaries of the radio jets. Projection effects could easily make the observed radial velocities of 200–300 km s^{-1} of this "backbone" (with respect to the apparent systemic velocity) consistent with the space velocities of roughly 500 km s^{-1} required for photoionization by thermal bremsstrahlung to dominate the spectrum in the region near the shocks and to account for the observed emission-line ratios (Dopita & Sutherland 1996). In what follows, we take as a working hypothesis that the high-velocity gas motions are the result of some direct or indirect action of the radio jet on the ambient gas.

We first consider one specific scenario in which the high gas velocities result indirectly from the action of the radio jet: entrained material, colliding with ambient dense regions, precipitates an intense episode of very localized star formation on one side of a comparatively large cloud. A superwind driven primarily by mass loss from O–B stars then expands preferentially in the direction of the steepest negative density gradient, and we see primarily either a blueshift or a redshift depending on our line of sight with respect to this expansion axis.

We can test the consistency of this picture by estimating whether the implied starburst mass is reasonable for *b*. From our Hγ and Hδ fluxes, we obtain an Hβ luminosity $L_{H\beta}=3\times10^{42}$ erg s^{-1} ($H_0=75$, $q_0=0$). From recombination theory (e.g., Osterbrock 1989), $L_{H\beta}=1.24\times10^{-25}M_pN_e$, where we have made the approximation that all of the emission comes from regions at a constant electron density N_e and total mass in protons M_p. We obtain $M_p=1.4\times10^{41}$ gm or $7\times10^7M_\odot$, assuming an electron density $N_e=300$ cm^{-3} (this value may well be too high for such a region, but anything lower will only increase the estimated mass). From the emission-line profiles, we measure a root-mean-squared velocity for the wind of 500 km s^{-1}. Using the mass M_p found above, we determine a kinetic energy for the ionized gas of 2×10^{56} erg. Leitherer *et al.* 1992 have estimated the power input from O–B star winds from a population of stars formed with a Saltpeter initial mass function and find that, for times up to a few 10^6 years, it is fairly constant at $\sim10^{34}$ erg s$^{-1}M_\odot^{-1}$. The total energy deposited from stellar winds over a 10^6-year period from an instantaneous starburst is then 3×10^{47} erg $M_\odot^{-1}$, and we require a starburst of $\sim10^9M_\odot$ to match the observed kinetic energy from bulk motions of the gas. We calculate the expected flux density at 3200 Å from the young stars after 10^6 years from the models of Bruzual & Charlot (1993). At this wavelength, the contribution from the nebular thermal continuum is almost independent of temperature over the relevant range. We find that the continuum from a $10^9M_\odot$ starburst would be a factor of ~15 greater than that remaining after removal of the nebular component.

This discrepancy could be softened and possibly removed by assuming higher densities in the emitting regions or a longer time span over which the necessary energy is input. But lifetimes of powerful radio sources [based on spectral aging of electrons in lobes (e.g., Alexander & Leahy 1987)] are estimated to be $\sim10^7$ years, and 3C 368 shows every indication of being relatively young. Furthermore, we have implicitly assumed 100% efficiency in converting the energy in stellar winds to bulk motions of the gas, and our assumption of an instantaneous starburst is unrealistic in the context of a 10^6-year time scale. We feel we can safely reject

starburst-generated superwinds as a plausible explanation for the high gas velocities in 3C 368.

We are left with some form of direct interaction between the radio jet itself (or thermal material entrained in it) and ambient external gas clouds to produce the high-velocity components. Entrainment alone seems unlikely to be the answer, since the one-sided velocity excursions on the N end of 3C 368 go to both higher and lower velocities. The interaction of radio jets with thermal plasmas is still poorly understood, and we can only put forward broad speculations on possibilities worth further exploration. One such possibility is prompted by the relative constancy of the velocities in the "backbone." If we are indeed seeing entrained material, one might expect velocities to increase along the jet, because of the continuuing acceleration of entrained cloudlets (De Young 1986). The constancy of the velocity implies that we are seeing only *freshly entrained* cloudlets at each point along the jet, presumably because the higher-velocity entrained material has been shocked and heated to temperatures that suppress the emission lines. Thus, the jet may contain much more thermal material than is readily apparent, and at higher velocities than we measure from the emission lines. While it is still not clear how an encounter of the jet with cold ambient material can produce the high-velocity 10^4 K gas we see, at least it is reasonable to suppose that bulk flows of thermal material at comparable or higher velocities could be present in the jet. In any case, we emphasize that any credible mechanism must be consistent with the one-sided nature of the observed outflows.

5. SUMMARY

We have confirmed the identification by Hammer *et al.* (1991) of the bright component *a* as a projected Galactic M dwarf star, and we have identified on our high-resolution IR image what we believe to be the true nucleus, lying about 1.″5 N of the M star.

From our spectra, we argue that the apparent correlation between the line intensity and the presence of large velocity excursions suggests that the mechanisms producing the line excitation and the bulk motions must be closely coupled. The localized high-velocity outflows seen in the emission lines are almost certainly due to some form of direct interaction between the radio jets and ambient gas clouds, although the specific mechanism remains unclear. Neither simple entrainment alone nor superwinds generated by jet-induced star formation seem consistent with our observations.

We extend the previous work of Dickson *et al.* (1995) and show that the nebular thermal continuum makes a significant (and usually dominating) contribution to the continuum alignment effect in 3C 368. Because any scattered contribution to the continuum of *b* in the restframe near-UV must be $\lesssim 20\%$, the absence of a detectible broad Mg II component can no longer be considered a serious objection to the presence of a hidden quasar nucleus in 3C 368.

Finally, we have some evidence to suggest that photoionization by high-velocity shocks may dominate the ionization of the extended gas. However, our results cannot be considered conclusive on this point, and, in any case, photoionization by a hidden quasar nucleus may play a role as well. Any photoionization by hot stars produced in starbursts must be comparatively minor.

As we mentioned at the outset, 3C 368 is an extreme object: it cannot be taken as representative of powerful high-redshift radio galaxies as a class. Even among $z \sim 1$ 3CR galaxies showing a strong alignment effect, there are major variations, probably reflecting differences in the relative importance of various physical mechanisms responsible for the alignment. In 3C 368, the correlation between the aligned continuum and the aligned emission-line components appears to be closer than usual. This is of course a natural consequence of the strength of the emission and the corresponding strength of the nebular thermal continuum. But the presence of strong emission itself probably reflects a situation in which most of the aligned material in 3C 368 is still involved in direct interaction with the radio jets; this in turn may point to its relative youth in an evolutionary sequence (Longair *et al.* 1995).

We are grateful to Malcolm Longair and Phillip Best, who generously supplied digital versions of their *HST* and VLA data; to Arjun Dey for a helpful discussion and for allowing us to mention the new polarization data he and his colleagues have obtained; to Ken Chambers, Bill Vacca, and George Lake for helpful discussions; and to the Thursday afternoon tea and journal club at the Institute for Astronomy, where an early version of this work was discussed. Much of the data presented was obtained at the W. M. Keck Observatory, which is operated as a scientific partnership between the California Institute of Technology and the University of California, and which was made possible by the generous financial support of the W. M. Keck Foundation. Wayne Wack and Tom Bida helped us make the most of the available time on Keck. We also thank the many people at the Institute for Astronomy who worked so hard to make the UH 88-inch telescope tip-tilt secondary a reality. A. S. thanks the NSF for partial support of this work under grant AST9221909.

REFERENCES

Alexander, P., & Leahy, J. P. 1987, MNRAS, 225, 1
Aller, L. 1987, Physics of Thermal Gaseous Nebulae, Astrophys. Space Sci. Library, vol. 112 (Reidel, Dordrecht)
Barthel, P. D. 1989, ApJ, 336, 606
Bruzual, G., & Charlot, S. 1993, ApJ, 465, 538
Chambers, K. C., Miley, G. K., & Joyce, R. R. 1988, ApJ, 329, L75
Chambers, K. C., Miley, G., & van Breugel, W. 1987, Nature, 329, 609
Chambers, K. C., Miley, G., & van Breugel, W. 1990, ApJ, 363, 21
De Young, D. 1986, ApJ, 307, 67
Dey, A., & Spinrad, H. 1996, ApJ, 459, 113
Dey, A., van Breugel, W., Graham, J., Spinrad, H., Cimatti, A., Hurt, T., & Antonucci, R. 1996, in preparation

di Serego Alighieri, S., Fosbury, R. A. E., Quinn, P. J., & Tadhunter, C. N. 1989, Nature, 341, 307
Dickinson, M., Dey, A., & Spinrad, H. 1996, in Galaxies in the Young Universe, edited by H. Hippelein (Springer, Heidelberg), p. 164
Dickson, R., Tadhunter, C., Shaw, M., Clark, N., & Morganti, R. 1995, MNRAS, 273, L29
Djorgovski, S., Spinrad, H., Pedelty, J., Rudnick, L., & Stockton, A. 1987, AJ, 93, 1307
Djorgovski, S., Weir, N., Matthews, K., & Graham, J. R. 1990, in Astrophysics with Infra-Red Arrays, edited by R. Elston (ASP, San Francisco), p. 112
Dopita, M. A., & Sutherland, R. S. 1996, ApJS, 102, 161
Hammer, F., Le Fèvre, O., & Proust, D. 1991, ApJ, 374, 91
Hook, R., & Lucy, L. 1994, in The Restoration of *HST* Images and Spectra. II, edited by R. Hanish and R. White,
Hook, R., Lucy, L., Stockton, A., & Ridgway, S. E. 1994, *ST-ECF Newsletter*, No. 21, p. 16
Lacy, M., & Rawlings, S. 1994, MNRAS, 270, 431
Leitherer, C., Robert, C., & Drissen, L. 1992, ApJ, 401, 596
Longair, M. S., Best, P. N., & Röttering, H. J. A. 1995, MNRAS, 275, L47
McCarthy, P. J., Spinrad, H., van Breugel, W., Liebert, J., Dickinson, M., Djorgovski, S., & Eisenhardt, P. 1990, ApJ, 365, 487
McCarthy, P. J., van Breugel, W., Spinrad, H., & Djorgovski, S. 1987, ApJ, 321, L29
Meisenheimer, K., & Hippelein, H. 1992, AAP, 264, 455
Netzer, H., Elitzur, M., & Ferland, H. 1985, ApJ, 299, 752
Osterbrock, D. E. 1989, Astrophysics of Gaseous Nebulae and Active Galactic Nuclei (University Science Books, Mill Valley, CA)
Rigler, M. A., Lilly, S. J., Stockton, A., Hammer, F., & Le Fèvre, O. 1992, ApJ, 385, 61
Scarrott, C. M., Rolph, C. D., & Tadhunter, C. N. 1990, MNRAS, 243, 5P
Scheuer, P. 1987, in Superluminal Radio Sources, edited by J. Zensus and T. Pearson (Cambridge University Press, Cambridge), p. 104
Spinrad, H. 1982, PASP, 94, 397
Spinrad, H., & Djorgovski, S. 1984, ApJ, 280, L9
Stockton, A., Kellogg, M., & Ridgway, S. E. 1995, ApJ, 443, L69

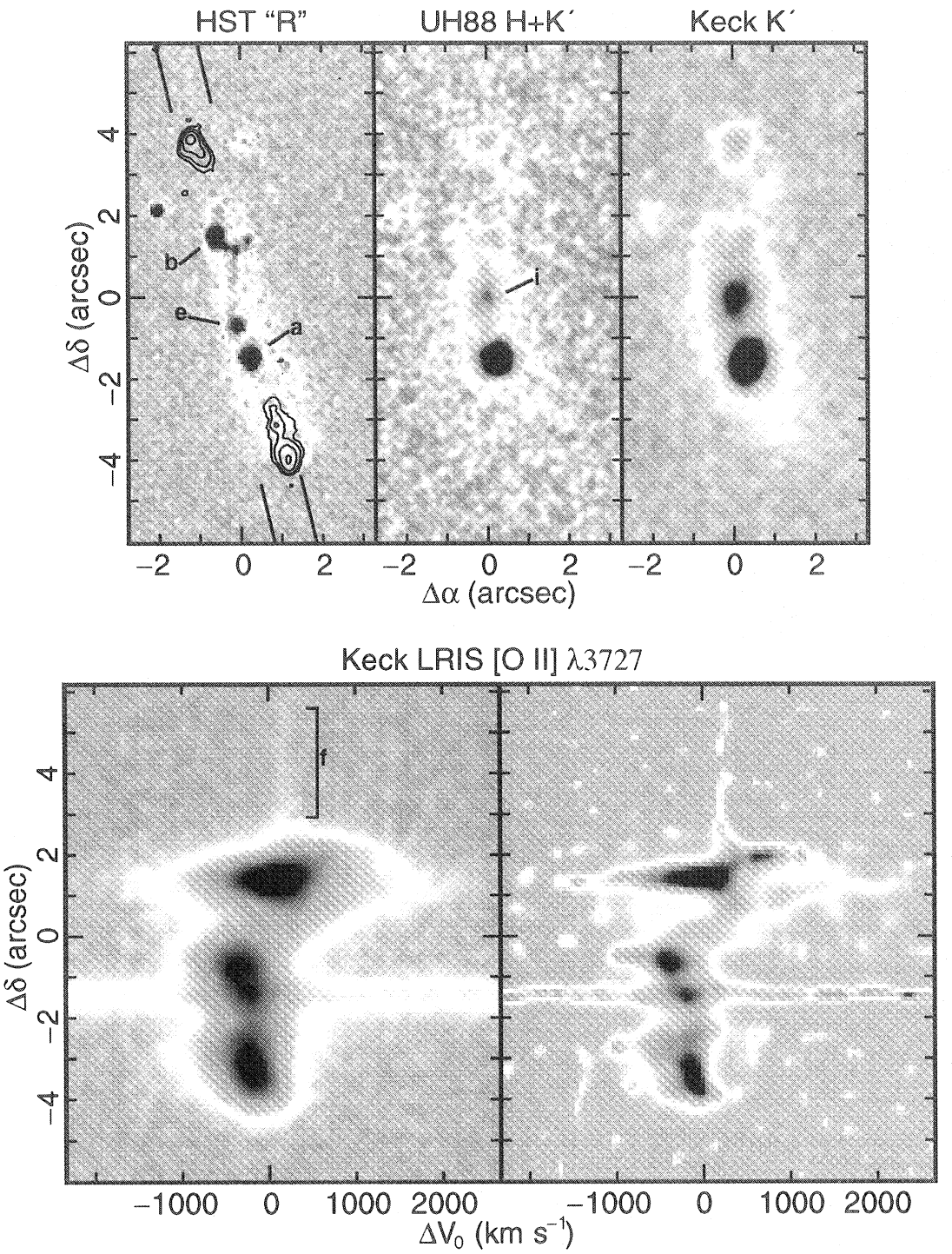

FIG. 1. Images and [O II] spectra of 3C 368. (top left) *HST* image. Both the image and the superposed 3.6 cm VLA radio contours are from Longair *et al.* (1995). The filter bandpass includes strong emission lines. The diagonal lines at the top and bottom indicate the position and width of our spectrograph slit. Three of the features discussed in the text are labeled. Component *d*, which represents the diffuse background, is not labeled, but it includes the region between *b* and *e* plus the region south of *a*. Component *f* is indicated in the spectral image below. The coordinate system has its origin at the position of the IR nucleus. (top middle) *H*+*K* image. The IR nucleus is labeled *i*. (top right) Keck NIRC *K*′ image. (bottom left) [O II] spectral image. The ordinate scale gives distance along the slit projected onto the declination axis to allow easier comparison with the images. (bottom right) [O II] spectral image, deconvolved to 0.″25.

Stockton *et al.* (see page 903)